Winter Storms in the Central Himalayas

Timothy J. LANG and Ana P. BARROS

Division of Engineering and Applied Sciences, Harvard University, USA

(Manuscript received 6 January 2003, in final form 20 November 2003)

Abstract

Based on observations from a hydrometeorological network on the eastern slopes of the Annapurna Range, nearly all the annual precipitation at low elevations (< 2000 m MSL) in Nepal is in liquid form, even during the winter. However, high elevations (> 3000 m MSL) can receive up to 40% of their annual precipitation as snowfall during the winter, with the highest altitude stations (~4000 m MSL and above) having the most total winter precipitation (which can exceed 100 cm). Significant snowstorms are associated with terrain-locked low-pressure systems that form when an upper-level disturbance passes over the notch formed by the Himalayas and Hindu Kush mountains (the so-called Western Disturbances), causing upper-level SW flow over central Nepal and orographically forced precipitation. Based on these results, a 30-year (1973–2002) climatology of these notch depressions is developed and reveals that significant interannual variability in central Himalayan winter storms exists. Weak but statistically significant correlation between notch depressions and the Polar/Eurasia teleconnection pattern was found, suggesting that the strength of the circumpolar vortex may affect the number of depressions passing through the Himalayan region. A typical snow event (11 February 2000) was the subject of an observational and modeling case study. Local precipitation (snow and rain) and other meteorological observations, as well as satellite (Meteosat-5 and TRMM) and NCEP/NCAR Reanalysis data were used, along with a cloud-resolving model with realistic topography. This study shows that significant wintertime precipitation only occurs in the central Himalayas when the large-scale flow evolves to a favorable geometry with respect to the mountains.

1. Introduction

While summertime precipitation in the central Himalayas, in particular Nepal, has recently received attention (Barros et al. 2000; Shrestha 2000; Lang and Barros 2002), the contribution of winter precipitation, especially snow, to annual totals is currently unknown. There also is a lack of understanding of the weather systems that are important for winter precipitation in the central Himalayas.

Despite the limitations of current scientific understanding, winter precipitation in this region is important. The rivers spawned in the Himalayas are tributaries to the Indus and Ganges Rivers, which are critical water supplies for hundreds of millions of people. Winter snowfall makes a significant contribution to these flows during the springtime melt, before the onset of the summer monsoon. Ramasastri (1999) estimated snowmelt contribution to various Indus tributaries in the range of 15–44%, and for Ganges tributaries 6–20%. Spring snowmelt becomes especially important in the case of a delayed monsoon onset, and would be expected to be a factor in pre-monsoon flooding and landslides.

In addition, many studies have documented an inverse relationship between Eurasian snow cover and the strength of the following summer

Corresponding author: Ana P. Barros, Dept. of Civil and Env. Engineering, Pratt School of Engineering, Duke University, 121 Hudson Hall, Box 90287, Durham, NC 27708, USA.
E-mail: ana.barros@duke.edu

monsoon in India (e.g., Hahn and Shukla 1976). Dickson (1984) demonstrated an increase in the level of statistical significance of this relationship when updated Himalayan snow cover data were included in the analysis. The basic physics of this mechanism is reduced land-sea thermal contrast based on increased surface albedo from snow cover, thus weakening the monsoon (Fu and Fletcher 1985; Li and Yanai 1996). In addition, Dey and Bhanu Kumar (1982) and Dey et al. (1985) showed that snow cover affected the timing of monsoon onset and withdrawal.

In the Himalayan regions of northwest India (e.g., Kashmir), the primary weather systems responsible for wintertime precipitation are the Western Disturbances, westerly upper-tropospheric synoptic-scale waves, that can undergo orographic capture and intensification as they pass over south central Asia (e.g., Gupta et al. 1999). While important for precipitation in northern India, it currently is unclear what role such storms have in causing winter precipitation in the central and eastern Himalayas.

Some studies have quantified monsoon (1 June–30 September) precipitation in the Nepalese Himalayas. In central Nepal, summertime rainfall totals can exceed 350–450 cm (Barros et al. 2000; Shrestha 2000; Lang and Barros 2002), with large variability (> 100 cm change) over short distances (~10 km) in the steep and varied terrain of the central Himalayas. Monsoon totals show no obvious dependence on altitude. Shrestha (2000) estimated that the summer monsoon accounts for 80% of the annual rainfall in Nepal. However, this study did not have access to snowfall estimates, and was lacking in precipitation measurements along high altitude ridges.

The present study seeks to accomplish three goals: 1) Gauge the climatic importance of winter precipitation at different elevations in the Nepalese Himalayas; 2) Identify, describe, and diagnose important weather systems and climatic patterns for winter weather; 3) Understand how these weather systems interact with the massive topographic barrier of the Himalayas and Tibetan Plateau to produce the observed precipitation. The first two goals will be approached via analysis of observations, while the third will be approached through the use of a numerical model.

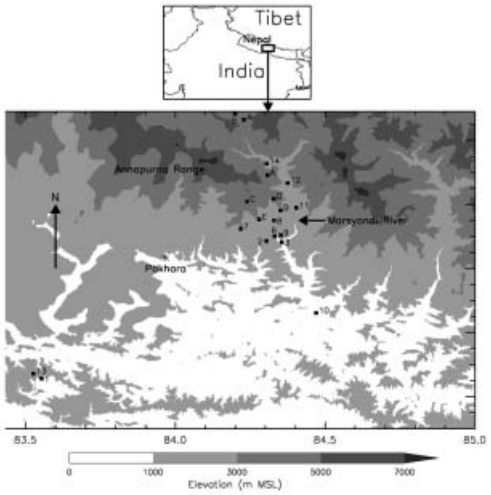

Fig. 1. The lower map is a topographic map of the Marsyandi River basin, showing locations of the meteorological stations in the network (letters and numbers; Tables 1 and 2). The 5 lettered stations have instruments to measure snowfall. Also shown are various landmarks in the region, including the city of Pokhara. The upper map shows the location of the network relative to southern Asia.

2. Data and methodology

2.1 Observations

a. Marsyandi network

The Marsyandi hydrometeorological network is shown in Fig. 1, with station information presented in Tables 1 and 2. There are a total of 20 stations, varying in altitude from 528 to 4435 m. The focus of the network is 3 southward-protruding high-altitude ridges, as well as adjacent valleys and areas in the dry regions north of the Annapurnas. Each station is equipped with at least one tipping bucket rain gauge, as well as a thermometer and a hygrometer. These instruments report observations every half hour, and the data are logged on site with electronic dataloggers, which must be serviced manually every few months. Six stations, including all of the snow-instrumented stations (see below), feature 10-m meteorological towers with additional instrumentation, including wind observations. The Telbrung station on the central ridge also makes several other observations, including solar radiation and soil moisture. For more information on the

Marsyandi network, see Barros et al. (2000), Lang and Barros (2002), and Barros and Lang (2003).

During the 1999–2002 winters, up to five stations (Danfedanda, Koprung, Rambrong, Sundar, Telbrung—lettered stations in Fig. 1) were equipped with instruments to measure snow depth and snow water equivalent. At each snow-equipped station, snow depth is measured by a sonic snow depth ranger, which is mounted on the tower at a level that is consistently above the snowpack. The measurement is taken and recorded instantaneously at local midnight. Measurement uncertainty is a least 1 cm. In addition, sonic ranger measurements are sensitive to drifting and settling snow, so sometimes snow depth changes are not necessarily attributable to precipitation or melting. For this reason it is difficult to identify snow events using only one station. Better confidence is obtained through identifying precipitation events based on consistent measurements at multiple stations.

Snow water equivalent (SWE) is measured by a gamma ray logger, which is installed at ground level and then covered by snowfall. This instrument requires 1–3 hours to make a proper measurement, and this cycle is timed so that the report comes at the same time as the sonic ranger. Uncertainty in measured SWE is 1.5 cm. SWE is much less sensitive to drifting and settling snow, so measurements typically are much less noisy than the sonic ranger (Dr. Jaakko Putkonen, personal communication, 2003). Using monthly snow depth measurements from a number of snow stakes placed around the Rambrong and Telbrung towers, a maximum error due to wind drift on the order of 2 cm was estimated. The Koprung station lacked a gamma ray logger, so only snow depth measurements were available from there.

Due to the noisiness of snow observations, it was difficult to accurately measure totals from individual snow events. This was particularly true for light snowfall. Thus, while a straight sum of rainfall from individual precipitation systems was suitable for rain gauge data, it is better to measure snowfall totals on a seasonal basis. Seasonal SWE totals were measured by summing from the minimum value (i.e., 0) to the maximum value over the wintertime period. At stations in which major melting events occurred between snowstorms during the winter (Telbrung during the 2000–01 and 2001–02 winters, Sundar during the 2000–01 winter), differencing between multiple minima and maxima was done. Snow depth data were used primarily to identify snowfall events. Rain gauges in the network were not heated, and were vulnerable to recording snowmelt that found its way into their buckets. Therefore, all measured rainfall at snow stations during the time when snow existed on the ground was considered snowmelt. These totals were subtracted from annual rainfall totals at snow stations to avoid double counting.

During the winter of 1999–2000, an avalanche collapsed the Danfedanda tower, so no data were available from that winter. In addition, the Rambrong tower was struck by lightning during the 2002 spring, wrecking the datalogger that contained the previous winter's snowfall data. Therefore, no data were available from Rambrong during the 2001–02 winter.

b. Satellite data

The European Meteorological Satellite Organization (EUMETSAT) maintains a geostationary meteorological satellite, Meteosat-5, above the Indian Ocean at 63°E longitude. This satellite makes visible (VIS), infrared (IR), and water vapor (WV) observations, similar to other geostationary weather satellites like GOES, and hourly infrared data were used to characterize the time history of weather systems in this study.

The Tropical Rainfall Measuring Mission satellite (TRMM; Kummerow et al. 2000), launched in November 1997, was used to characterize the instantaneous spatial (horizontal and vertical) structure of precipitation systems in the Himalayas during overpasses, which occur approximately daily in this study's region. The sensors of interest included the Precipitation Radar (PR) and TRMM Microwave Imager (TMI), both described in Kummerow et al. (1998). TRMM does not capture the time history of individual precipitation systems due to its sampling frequency, and its ability to detect snowfall is hampered by its minimum reflectivity factor threshold of 18 dBZ. Based on summertime observations, TRMM has some trouble detecting rainfall at altitudes greater

than 2000 m MSL, and consistently underestimates rain rates relative to gauges in the central Himalayas (Barros et al. 2000).

c. NCEP/NCAR reanalysis

The NCEP/NCAR Reanalysis (Kalnay et al. 1996) was used to characterize the large-scale environment in this study. Reanalysis data were available at 6-hour intervals, 2.5° horizontal resolution, and 12 vertical levels in the range 1000–100 hPa. The reanalysis compared well with summertime radiosonde data taken from the Himalayas (Barros and Lang 2003), particularly with regard to upper-level winds (500 hPa and above). Precipitable water, however, is considerably underestimated in this region, at least during the summer. Therefore, moisture flux estimates cannot be used to investigate precipitation potential.

2.2 Model

The model used for our numerical experiments was a regional model originally introduced by Clark (1977). This is a non-hydrostatic model with a terrain-following coordinate system, which has undergone substantial upgrades since its inception (Clark 1979; Clark and Farley 1984; Smolarkiewicz 1984; Klaassen and Clark 1985; Smolarkiewicz and Clark 1986; Clark and Hall 1991; Bruintjes et al. 1994; Clark and Hall 1996). The most recent major update has been the implementation of code to take advantage of MPI-based multiprocessing, for rapid completion of simulations. The model has been successfully applied in the study of various small-scale and mesoscale weather phenomena in regions of complex topography, including wintertime situations (Bruintjes et al. 1994; Reinking et al. 2000).

The model was run as a single domain with 23.3-km horizontal resolution (122×122 gridpoints) and 62 vertical levels (spaced 75–800 m stretching with height). The approximate latitude and longitude range of the domain was 15–40°N and 68–93°E, respectively. This simulation was initialized with large-scale spatially and temporally varying data, derived from 1.125° ECMWF analysis data that are available at 6-hour intervals. The simulations were based on data from 10–12 February 2000 (UTC time), which contained a representative snow event (11 February). A detailed explanation of the hydrometeorological conditions that define a representative snow event will be provided in Section 4.

The simulation was initialized at 0000 UTC on 11 February and run for 24 hours. Sensitivity tests revealed that the first 3–4 hours of simulation time were affected by spin-up. Therefore, we focused our model analysis after this time period. A modified Kessler (1969) warm rain bulk microphysics parameterization, which predicts the mixing ratios of cloud liquid water and rainwater, was used to characterize microphysics. The Coriolis effect was included, but for simplicity radiation and ice physics were not included in the simulation. The goal of this simulation was to investigate orographic effects on the spatial and temporal distribution of precipitation during snow events, and the simplified setup was sufficient for this task.

3. Observational results

3.1 Precipitation statistics

Table 1 shows annual precipitation for all Marsyandi snow-instrumented ridge stations, and Table 2 shows the same for non-snow-instrumented stations. The data shown correspond to the 1 May–30 April totals for 1999–00, 2000–01, and 2001–02. Snow is reported as total snow water equivalent (SWE). The annual rainfall totals show significant variability, both spatially and interannually. As an example, in 2000–01 the windward Telbrung station received 520 cm of rain while the Monastery station in the lee of the Annapurnas received only 30 cm. However, rainfall at Telbrung varied as much as 80 cm from year to year. Based on the 1999 and 2000 totals presented in Barros et al. (2000) and Lang and Barros (2002), the monsoon period (1 June–30 September) comprises the vast majority of the annual rainfall at every station, on average 80–85%. The consistently wettest stations are stations on the central and western ridges of the network (Ganpokhara, Pasqam Ridge, and Telbrung), which lie in the elevation range 2100–3200 m MSL (Tables 1 and 2).

From the snow statistics it can be seen that precipitation in the form of snow tends to increase with elevation, when comparing Rambrong and Danfedanda totals with those from lower altitude snow stations such as Telbrung. However, since the number of snow stations is so few it cannot be confirmed that snowfall

Table 1. 1 May–30 April annual precipitation totals for the stations within the Marsyandi network that have snow instrumentation, broken down by rain and snow water equivalent. All precipitation values in cm. See Fig. 1 for locations. NA: Not available. *Incomplete record.

	A. Danfedanda	B. Koprung	C. Rambrong	D. Sundar	E. Telbrung
Elev. (m MSL)	3987	3133	4435	3823	3168
99–00 Rain	227.8	238.2*	322.3	337.3	452.8
99–00 Snow	NA	NA	105.8	76.5	22.3
99–00 Total	227.8	238.2*	428.1	413.8	475.1
99–00 Snow Frac	NA	NA	24.7%	18.5%	4.7%
00–01 Rain	152.2*	385.1	352.5	355.0	519.5
00–01 Snow	103.2	NA	131.3	52.3	26.6
00–01 Total	255.4*	385.1	483.8	407.3	545.1
00–01 Snow Frac	40.4%*	NA	27.1%	12.8%	4.9%
01–02 Rain	179.8	368.0	216.3*	309.6	440.3
01–02 Snow	100.3	NA	NA	48.5	32.1
01–02 Total	280.1	368.0	216.3*	358.1	472.4
01–02 Snow Frac	35.8%	NA	NA	13.5%	6.8%

depends solely on elevation. Regardless, snowfall has a mitigating effect on annual precipitation differences, causing high-altitude station totals to become closer in value despite significant differences during the rest of the year (in particular during the summer monsoon). For example, in 1999–00, annual (snow plus rain) precipitation differences between the three ridge stations (Rambrong, Sundar, and Telbrung) were 61.4 cm or less despite annual rainfall differences as high as 130.5 cm.

It follows from this that snowfall plays an important role in annual precipitation at higher elevations. Indeed, the fraction was approximately 25% at Rambrong (1999–00 and 2000–01), and higher than 35% at Danfedanda (2001–02), which lies just on the lee (north) side of the Annapurnas. In addition, SWE totals can exceed 100 cm at these highest stations. This is striking as winter precipitation at low elevations (< 2000 m MSL) is generally less than 20 cm over the entire January–March period on the south-facing (upwind) slopes.

Total SWE values showed significant interannual variability, with increases on the order of 20–30% at the central ridge stations (Ram-

Table 2. 1 May–30 April annual rainfall for stations within the Marsyandi network that lack snow instrumentation. All rain values in cm. See Fig. 1 for locations. [1]Added after 1999 monsoon. NA: Not available. *Incomplete record.

Station	Elev. (m MSL)	99–00 Rain	00–01 Rain	01–02 Rain
1. Bortung	1072	174.7	158.9	130.4
2. Ganpokhara	2120	471.8	428.1	407.0
3. Khudi	820	291.2	469.3	300.6
4. Monastery[1]	3562	NA	30.4	NA
5. Nargaon[1]	4220	NA	41.3	NA
6. Paiyu Khola[1]	993	NA	412.5	357.4
7. Pasqam Ridge[1]	2950	NA	431.2	478.5*
8. Probi[1]	1495	NA	406.2	334.7
9. Purano Village	1787	NA	369.1	157.6
10. Purkot	528	181.8	147.5	157.2
11. Syange	1200	66.6*	273.5	276.3
12. Tal	1358	163.3	102.3*	151.5
13. Tansen	1521	185.0	203.9	173.6
14. Temang	2760	176.0	124.8	128.5

brong and Telbrung) during 2000–01, but about a one-third decrease at the eastern ridge station of Sundar. Indeed, Sundar (3823 m MSL) showed a decreasing trend in SWE during the past three years, while Telbrung (3168 m MSL) saw increasing SWE. SWE at Danfedanda (3987 m MSL) was stable the past two years.

Figure 2 shows time series of snow depth, SWE, and temperature at available snow stations for the three winters 1999–2002. The plots provide more insight into the interannual variability observed in Tables 1 and 2, and also reveal significant intraseasonal variability. Most striking are the impacts of seasonal temperature differences, particularly at borderline rain/snow stations like Telbrung. In 1999–00, the station generally stayed cold enough to have a constant snowpack from early January to the end of March (average Jan–Mar temperature was ~0°C). The 2000–01 winter was much warmer, however (~2°C warmer at Telbrung during 1 January–31 March), and Telbrung snowpack was intermittent and did not remain much past February. The 2001–02 winter was intermediate, with a consistent yet variable snowpack at Telbrung for a month, yet no snow remained after February. In general, the higher the elevation of the station, the more consistent is the snowpack during the winter season.

Another result from Fig. 2 is the major differences in snow density among the three winters. The 1999–00 winter was the coldest on average (by up to 2°C) of the three, with lower snow density (~0.1–0.2 g cm^{-3} lower; SWE divided by snow depth) and much deeper snowpacks. Snow depth differences were as large as 100 cm at Rambrong (1999–00 vs. 2000–01). Note also the later peak in snow depth during 2000–01 at Rambrong. Thus, despite the reduced snow depths in the past two seasons, the increased snow densities explain the increasing trends in SWE observed at both Rambrong and Telbrung. The 2000–01 season featured more snowfall prior to the primary January–March period (as well as a later start for major snowpack development), while most of the snow in 2001–02 fell during three major events. The high interannual variability in snowpack is consistent with observations in the Khumbu/Everest region in the eastern Himalayas, where the number of days with snow cover shows large year-to-year changes (Ueno et al. 2001).

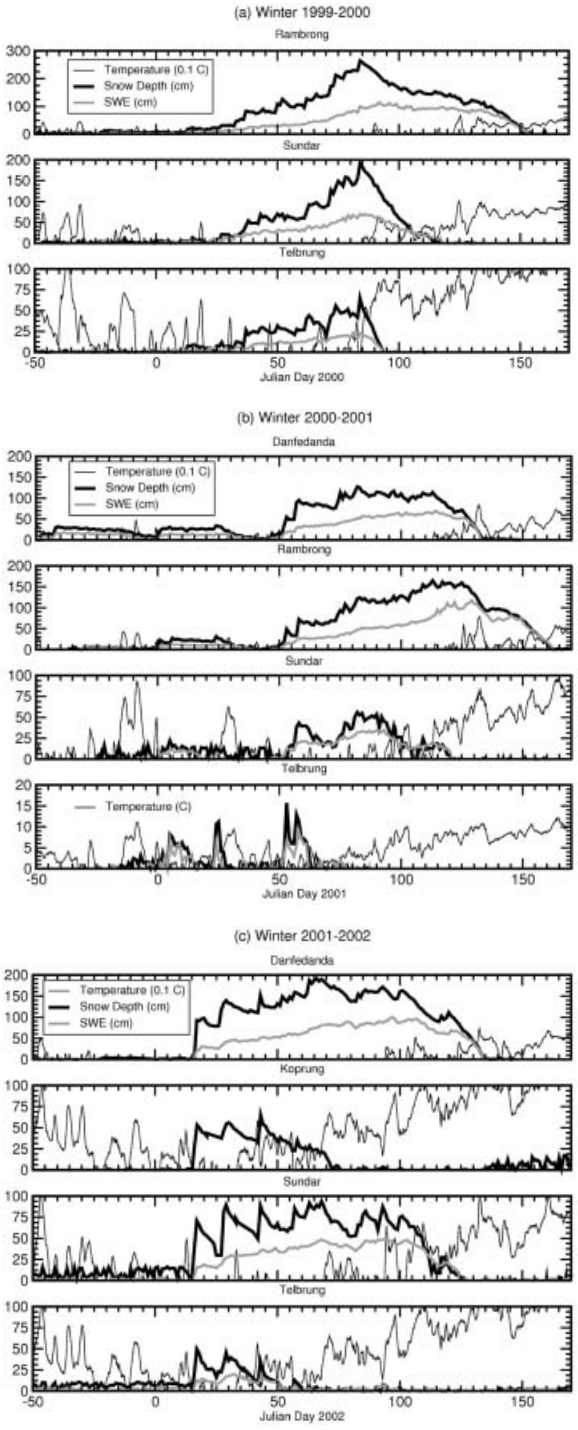

Fig. 2. Time series of snow depth, SWE, and temperature at available snow stations for three winters. (a) 1999–00. (b) 2000–01. (c) 2001–02. Temperatures below 0°C are not shown for scale reasons, as well as to emphasize potential melting events.

3.2 *Role of Western Disturbances*

Based on current knowledge of winter weather over northern India (e.g., Gupta et al. 1999), we hypothesize that Western Disturbances may be important for snowfall in the central Himalayas. Figure 3 shows time series of network snow depth, and 500 hPa geopotential height averaged over the region 70–75 E, 30–32.5 N (covering the Himalayan-Hindu Kush notch) for the three winters: January–March 2000 (a), 2001 (b), and 2002 (c). The 30-year (1973–2002) mean for these three months has been subtracted from each year's geopotential time series, and plus or minus the 30-year standard deviation also is shown. Clearly, snow depth increases correspond to below-average geopotential heights in the notch, despite the fact that the notch is ~10 degrees in longitude to the west of the network. This effect was most dramatic during the 2002 winter with its three deep depressions and three big snowfall events. Also note the large snowfalls in late February 2001. Interestingly, the intensity of the depression was not necessarily linked to total snowfall, with deep storms like mid-January 2000 providing only a few cm of snow, while the weaker depressions in late February 2001 were responsible for 10 s of cm of snow. Timing of snow during the depression also was variable.

Western Disturbances/notch depressions set up a favorable large-scale environment for snowfall in the central Himalayas, through the establishment of SW flow against the barrier. Locally, the amount of snow realized depends on other (likely mesoscale) factors. In particular, cross-barrier flow and moisture flux should determine snow yields. However, because our ultimate objective is to elucidate the relationship between local snowstorms qualitatively with larger synoptic events like Western Disturbances, we opted instead to use notch geopotential in our analysis. In addition, given the limitations of the Reanalysis in this region, reliable quantitative comparisons such as those conducted by Ohsawa et al. (2000) cannot be made between Reanalysis winds and snowfall amounts (Barros and Lang 2003).

Snow days in central Nepal were identified quantitatively as days in which three of the following four circumstances occur at the Marsyandi network: 1) ≥1 cm snow depth increase

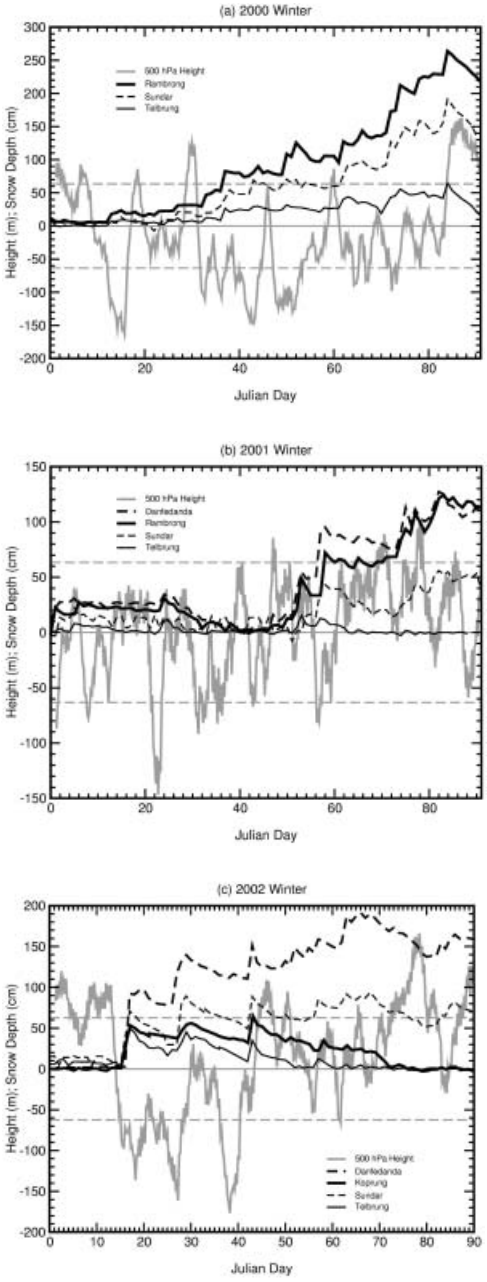

Fig. 3. Time series of network snow depth and 500 hPa geopotential height averaged over the region 70–75 E, 30–32.5 N (covering the Himalayan-Hindu Kush notch) for the three winters: January–March 2000 (a), 2001 (b), and 2002 (c). The 30-year (1973–2002) mean for these three months has been subtracted from each year's geopotential time series, and plus or minus the 30-year standard deviation (dashed lines) also is shown.

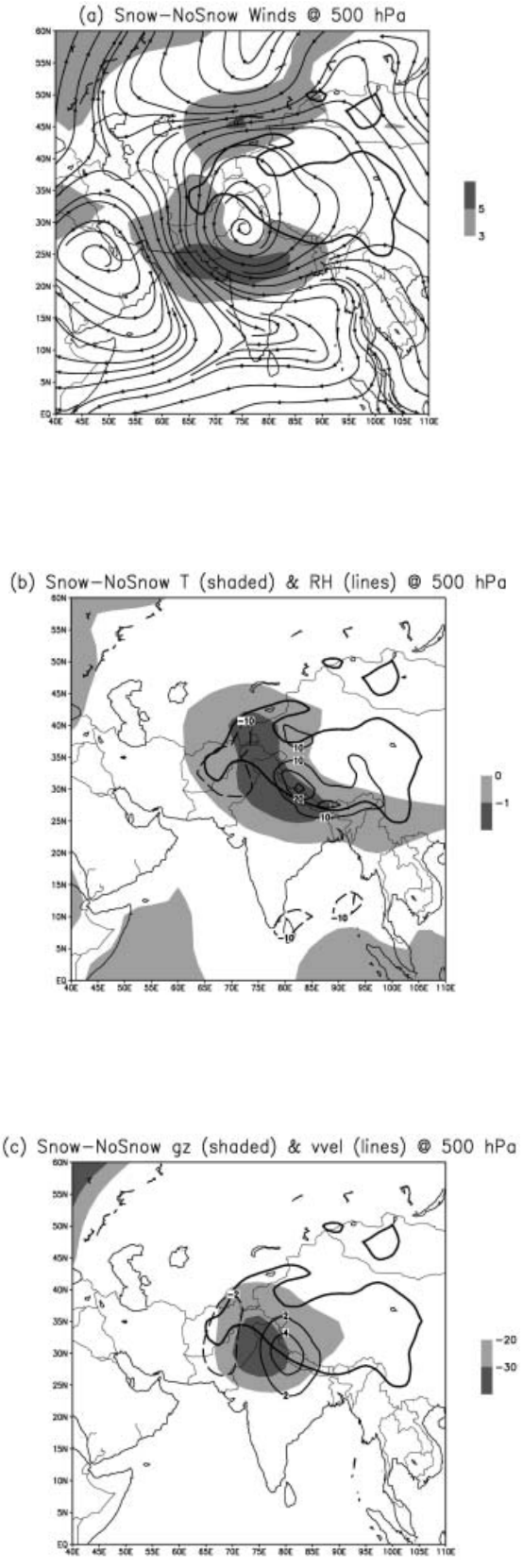

at Rambrong; 2) ≥1 cm of snow depth increase at Sundar; 3) ≥1 cm snow depth increase at Telbrung; or 4) ≥1 mm of rainfall at Ganpokhara. For 2002 Danfedanda was substituted for Rambrong due to the lack of data at the latter station. Based on these criteria, 19 snow days were identified in January–March 2000, 9 in 2001, and 16 in 2002. Reanalysis fields were averaged for the 24-hour periods associated with each snow day (starting at 0000 UTC). These snow-day values were differenced with non-snow-day fields for January–March 2000–2002, and the results are shown in Figs. 4 (horizontal cross-section at 500 hPa) and 5 (vertical cross-section at 27.5 N).

Analysis of the data indicates that snow days are associated with increased cyclonic flow and lower geopotential heights in the notch region, and enhanced westerly flow over northern India. In addition, snow days feature lower temperatures, higher relative humidities, and upward vertical motion over most of the western and central Himalayas. All of these tendencies are conducive to snowfall in the central Himalayas. The vertical cross-sections (Fig. 5) support these inferences, and also suggest that the effects extended throughout much of the troposphere. There is, however, large variability in these fields (high coefficient of variation). Analyses of many different individual snow days (not shown), as well as Fig. 3, imply that the high variability is associated with large differences in relative strength and locations of the depressions, not the lack of notch depressions themselves. In summary, heavy snowfall in the central Himalayas is unambiguously related to the presence of orographically captured depressions in the notch formed by the Hindu Kush

Fig. 4. Horizontal cross-sections at 500 hPa of NCEP/NCAR Reanalysis fields for snow days minus non-snow days for January–March 2000–02. (a) Wind speeds (shaded; m s^{-1}) and streamlines. (b) Temperature (shaded; K) and relative humidity (lines; %). (c) Geopotential (shaded; gpm) and vertical velocity (lines; hPa h^{-1}; upward motion is positive). Also shown in each plot are political boundaries (gray lines) and the 2000-m terrain contour in the reanalysis model (black lines).

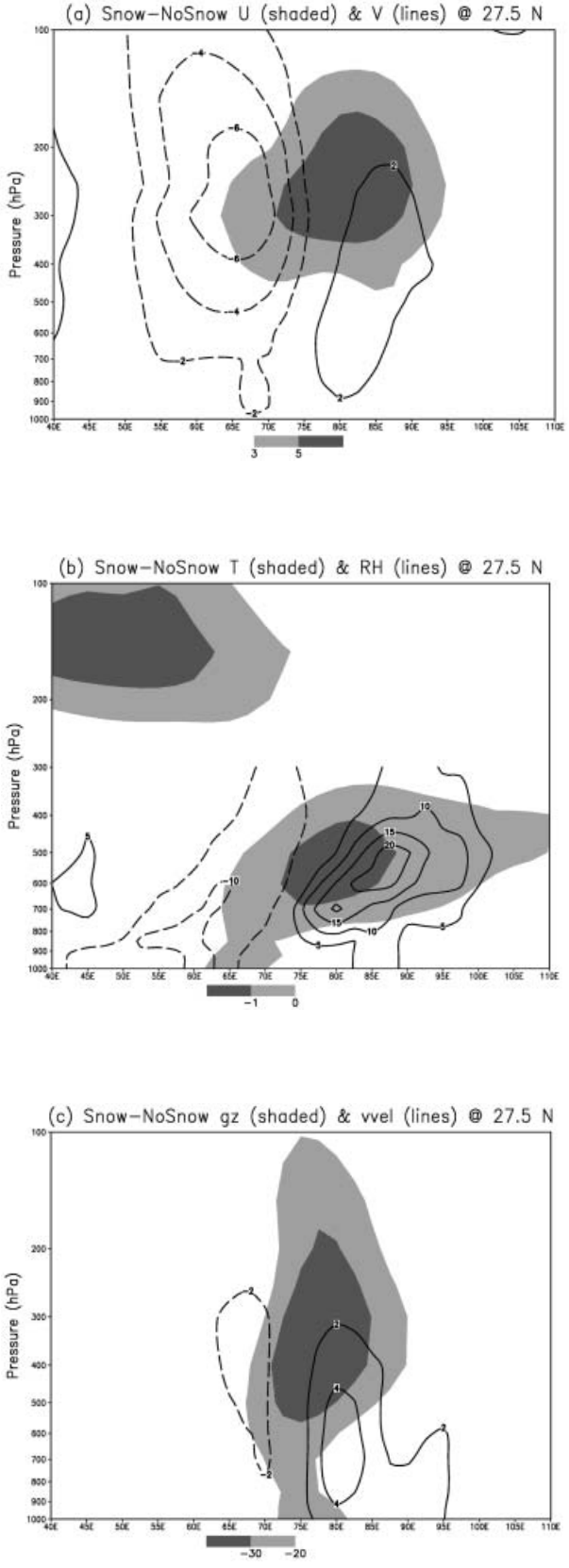

and the Himalayas; i.e., the so-called Western Disturbances responsible for winter precipitation elsewhere in the region, including northern India and Kashmir.

3.3 Depression climatology

Snowfall data for the Marsyandi network are available only for the past 3 winters (1999–2002), so in order to diagnose longer-term interannual variability a proxy of snowfall is required. Given the strong relationship between winter snowfall and the presence of notch depressions, a climatology of these depressions is appropriate. Note that snowfall amount does not correspond well to depression strength (Fig. 3). Yet, based on the observed characteristics of the synoptic fields during snow days, it is reasonable to suspect that years with large numbers of depressions, coupled with cold temperatures, would feature larger snow depths and possibly more accumulated SWE, when compared with warmer and less active years.

Figure 6 shows yearly time series (covering 1973–2002) of mean Jan–Mar 500 hPa geopotential height in the notch region (70–75°E, 30–32.5°N, as above), as well as 500 hPa temperatures averaged over the region 82.5–85°E, 27.5–30°N, which encompasses the 4 reanalysis grid points closest to the Marsyandi network. In addition, for each of these variables there are two more time series. The first, "events", gives the number of individual times per season the variable remained below 1 standard deviation from the 30-year mean for at least 1 consecutive day. The second, "time", gives the total number of days per season the variable remained below 1 standard deviation, whether

Fig. 5. Vertical cross-sections at 27.5 N of NCEP/NCAR Reanalysis fields for snow days minus non-snow days for January–March 2000–02. (a) U (shaded; m s^{-1}) and V (lines; m s^{-1}) wind speeds. Positive is westerly (U) or southerly (V). (b) Temperature (shaded; K) and relative humidity (lines; %). Moisture data are not defined above 300 hPa. (c) Geopotential (shaded; gpm) and vertical velocity (lines; hPa h^{-1}; upward motion is positive). The Marsyandi network resides in the region 80–85 E.

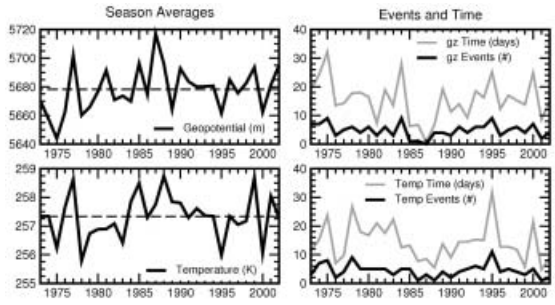

Fig. 6. Yearly time series (covering 1973–2002) of mean Jan–Mar 500 hPa geopotential height in the notch region (70–75 E, 30–32.5 N), as well as 500 hPa temperatures over the region 82.5–85 E, 27.5–30 N. Also shown are time series of low geopotential and temperature events (number of individual times per season the variable remained below 1 standard deviation from the 30-year mean for at least 1 consecutive day) and time (total number of days per season the variable remained below 1 standard deviation).

consecutive or not. Taken in concert, these variables provide information on the amount of potential snow days per season (low pressure in the notch combined with cold temperatures in the central Himalayas). While it would be very difficult to invert the problem and estimate snowfall in each season, these indices allow us to distinguish with confidence very active years from very inactive years.

The interpretation of Fig. 6 is started by examining the past 3 seasons (Jan–Mar 2000–2002), and diagnose the large-scale differences between these years and how they may have impacted the snowfall totals. From the discussion of Fig. 2, the Jan–Mar 2000 period featured less dense snow, higher total snow depths, and generally longer periods of snow on the ground than other years. From Fig. 6, the Jan–Mar 2000 period featured lower average geopotential height, lower average temperatures, and more deep depressions and cold outbreaks (both in terms of events and time) than the following two seasons. These large-scale observations are consistent with the low-density but plentiful snowfall that occurred in 2000. By contrast, Jan–Mar 2001 had higher geopotential and temperature, along with fewer low temperature and depression events, compared to adjacent years. This also is consistent with the shallow, wet snowpacks that occurred that year. Jan–Mar 2002 was mixed, with the highest geopotentials of the three years, but colder temperatures than 2001, in agreement with its placement between 2000 and 2001 in terms of total snow depth.

Based on the correspondence between low average geopotentials and temperatures, along with high numbers of cold and depression events, the years most likely to have featured similar snowfall to 2000 are 1975, 1984, and 1995. By contrast, years like 1981 and especially 1987 most likely saw very light snowpacks in the central Himalayas. These estimates require verification by other datasets, however.

We performed 30-year correlations between seasonal (January–March) averages of indices such as SOI and notch geopotential seasonal average, number of low geopotential events, and time duration under one standard deviation. All of these correlations were very low and statistically insignificant, with the exception of weak but statistically significant correlations (at 95% level, the correlation coefficient r is 0.361 for time and 0.344 for events) between notch geopotential and the Polar/Eurasia teleconnection pattern index. Information on this climate index can be obtained from the following website address: http://www.cpc.ncep.noaa.gov/data/teledoc/poleur.html. The Polar/Eurasia pattern is the most prominent mode of low-frequency variability during December and February in the Northern Hemisphere, reflects major changes in the strength of the circumpolar circulation, and reveals the accompanying systematic changes that occur in the midlatitude circulation over large portions of Europe and Asia, according to the NOAA Climate Prediction Center.

In essence, a stronger pattern means a stronger circumpolar circulation, which would be associated with larger numbers of upper-level disturbances passing through Asia. Thus, a physical link between the circumpolar circulation and Western Disturbance activity is plausible. However, location of the oncoming upper-level disturbance relative to the Tibetan Plateau (north or south) should be a major factor as well, as orographic capture of oncoming

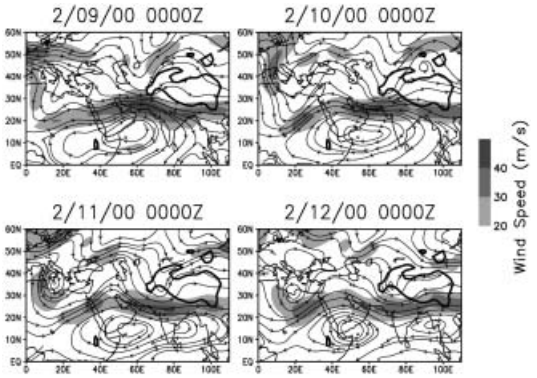

Fig. 7. Streamlines and wind speeds at 500 hPa from the NCEP/NCAR Reanalysis, for 0000 UTC on 9–12 February 2000.

depressions cannot occur if the disturbance is well north of the Plateau. It is extremely difficult to predict this latter effect, however, except on a case-by-case basis.

4. Case Study—11 February 2000

4.1 Observations

The typical meteorological scenario associated with snow events in the central Himalayas is best demonstrated with a case study. The case of interest is 11 February 2000, which featured snow depth increases at all stations in the range 5.5–22.2 cm (snow density 0.25–0.5). In addition, the Ganpokhara station, at a slightly lower elevation (2120 m MSL) along the central ridge, received 4.7 mm of rainfall scattered between 0600 and 1800 UTC. The synoptic situation is presented in Fig. 7, which shows 500 hPa streamlines and wind speeds from the NCEP/NCAR Reanalysis, for 0000 UTC on 9–12 February. This is a classic example of the Western Disturbance storms reviewed by Gupta et al. (1999) and Sikka (1999). Early on in the event, there is a deep trough running up against the west side of the Tibetan Plateau, coupled with strong wind speeds (> 30 m s^{-1}) associated with the north portion of an anticyclone of the southeast coast of the Arabian Peninsula. As the trough impacts the plateau, it splits into a northern and southern half. The northern portion of the trough continues passing along the northern side of the plateau, while the southern trough remains captured in the notch formed by the western Himalayas and the Hindu Kush mountains (the latter reside primarily in Afghanistan). During the lifecycle of the system the strong westerlies over South Asia continue blowing against the Himalayas, suggesting that orographic lifting plays an important role in the regional circulation (particularly at 500 hPa where the winds are less susceptible to blocking).

The development of these Western Disturbances, or notch depressions, is an interesting topic but will not be addressed in depth here. One factor that may be important for the orographic capture of these depressions is the interplay between leeside cyclogenesis, possibly due to vortex stretching, and the topographic barrier formed by the western Himalayas, which should reduce eastward propagation of the system. Regardless, the synoptic environment is conducive to the development of upper-level southwesterly flow over the central Himalayas.

Meteosat-5 data show interesting cloud structures associated with this storm. Figure 8 shows IR images at 0000 (a) and 1100 UTC (b) on 11 February. The latter time period is during precipitation at the Ganpokhara station, and presumably snow at higher elevation stations (> 3000 m MSL). At 0000 UTC, there is a large area of clouds pushed against the western Himalayas, up into the Kashmir region of northern Pakistan and India. Satellite animations reveal these clouds to be orographically generated, as their creation regions are fixed in space along the mountains. Meanwhile, there is a southward-protruding linear structure consisting of low clouds that propagates eastward along the mountains and northern Indian plains. The Marsyandi network is on the eastern boundary of the orographic clouds at 0000 UTC, but by 1100 UTC the southward protruding clouds are passing through the network's vicinity and into Bangladesh and NE India, and the orographically generated clouds have spread into the central and eastern Himalayas.

TRMM Precipitation Radar data reveal more details of the structure of the southward-protruding cloud systems. Figure 9 shows horizontal and vertical cross-sections of radar reflectivity factor for overpasses from 1634 UTC on 10 February 2000 (a), and from 1032 UTC on 11 February (b). Figure 9a shows signifi-

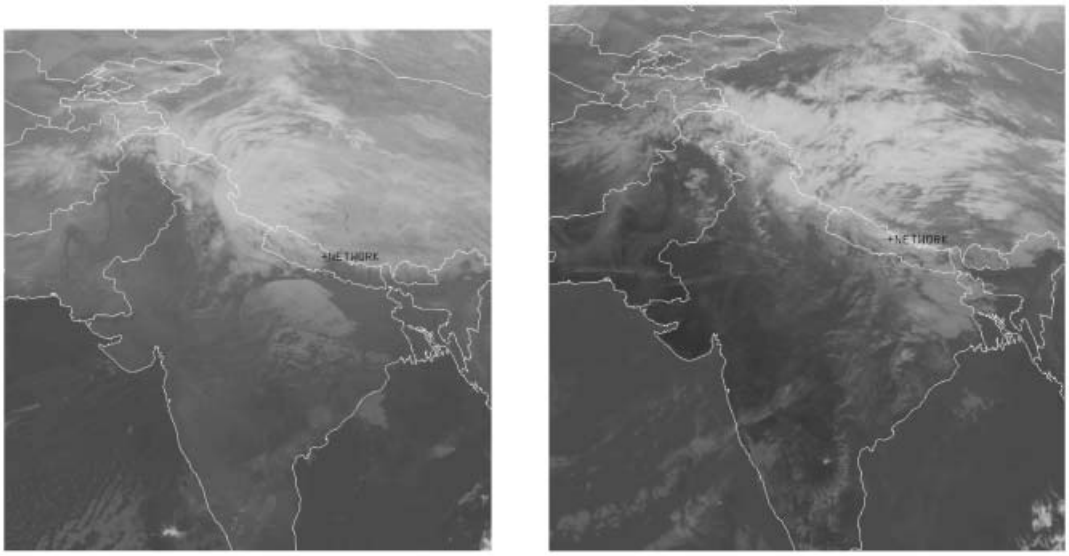

Fig. 8. Meteosat-5 IR images at 0000 (a) and 1100 UTC (b) on 11 February 2000.

cant widespread precipitation over the western Himalayan foothills, centered on a SW-NE-oriented linear convective feature. The entire system is shallow, not extending much over 6 km MSL in height, and often lower. The next day (Fig. 9b), during precipitation at Ganpokhara, the southward-protruding precipitation system consists of a number of isolated, shallow convective cells. Note that the PR coverage swath from this TRMM overpass unfortunately

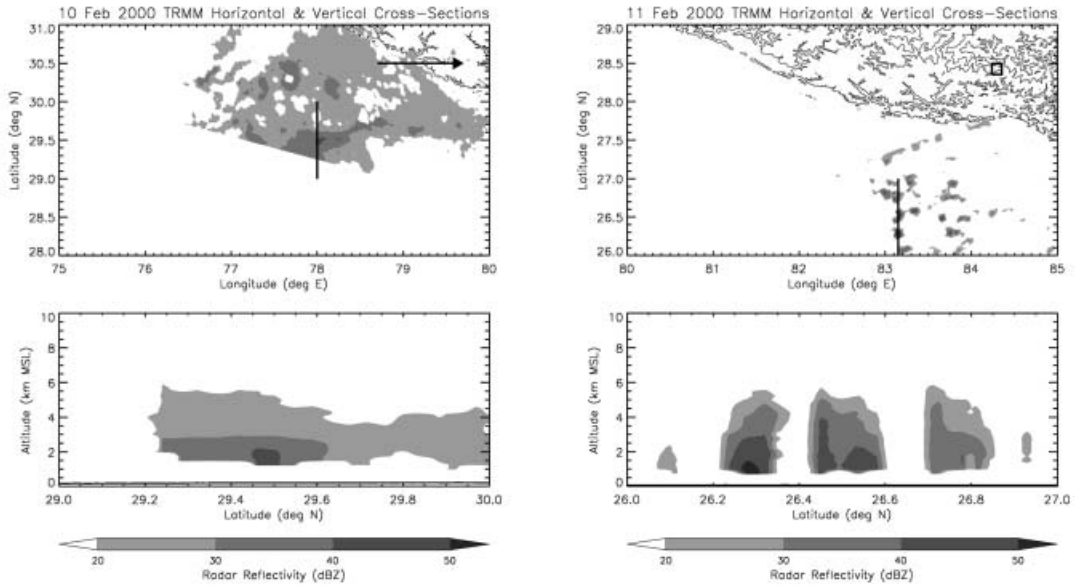

Fig. 9. Near–surface and vertical cross-sections of TRMM PR radar reflectivity factor for overpasses from 1634 UTC on 10 February 2000 (a), and 1032 UTC on 11 February Arrow points to the Marsyandi network that is far west to show in the figure. (b) The thick black line in the horizontal cross-section shows the location of the respective vertical cross-section, while the black box shows the approximate spatial extent of the Marsyandi snow stations.

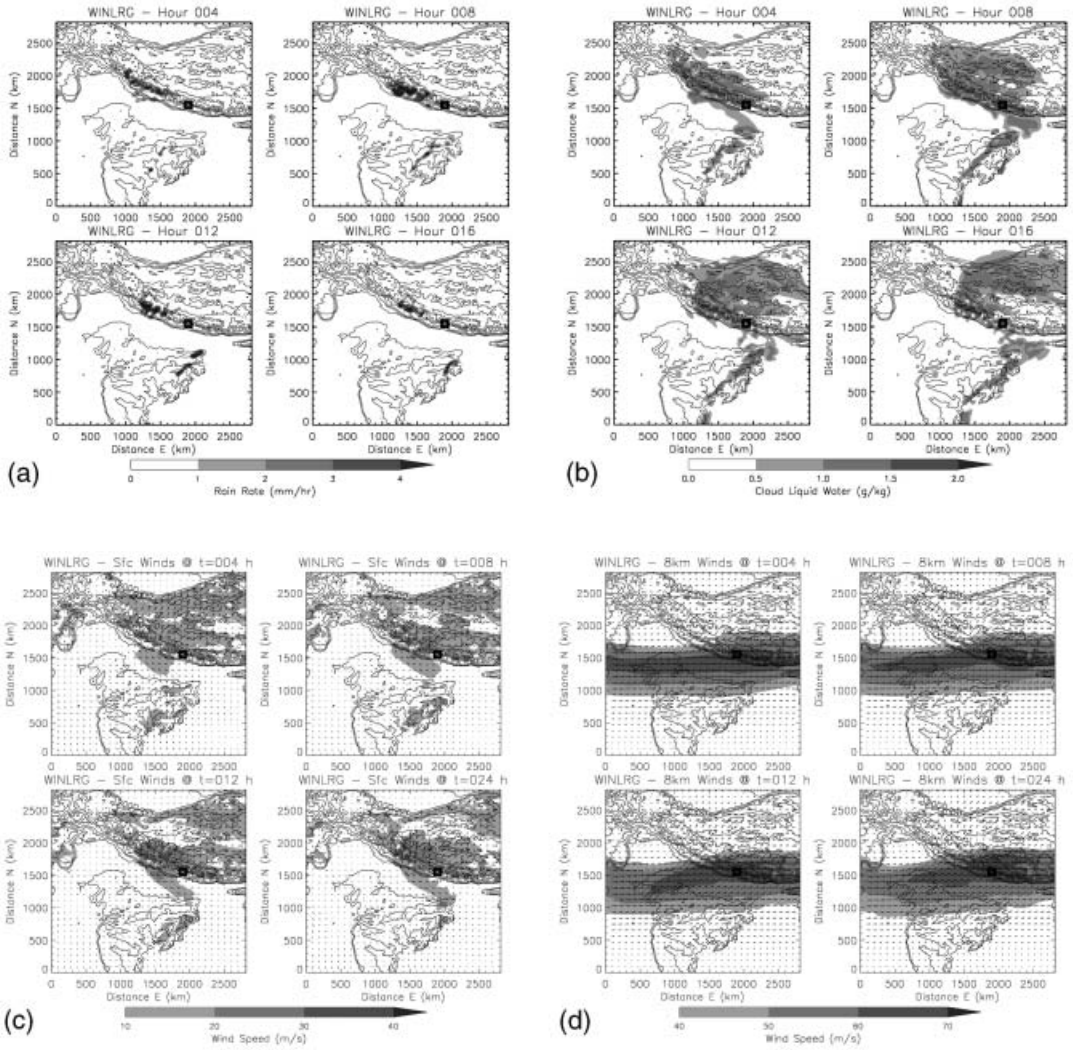

Fig. 10. Plots of various model simulation fields at 4 different times. Terrain contours (black curves) are 250 m, 500 m, 1000 m, and then spaced every 1000 m after that up to 8000 m MSL. (a) Surface rain rate. (b) Maximum cloud liquid water in the vertical column. (c) Surface winds. (d) Horizontal winds at 8 km MSL.

does not cover the Marsyandi network, so it is unclear to what extent the shallow convection contributed to precipitation at the network. The general outline of synoptic, cloud, and precipitation features associated with the 11 February snowfall event is typical of many snowstorms at the Marsyandi network.

4.2 Modeling

Results from the numerical simulation (termed WINLRG) are shown in Fig. 10. Note that the domain of the simulation was very large and extended over the ocean (portions of the Arabian Sea and Bay of Bengal); in the model this was treated as flat land with elevation 0 m MSL (i.e., ocean-atmosphere interactions were not considered).

In Fig. 10a, surface rainfall is important in two regions: along the south slopes of the Himalayas, and along a SW-NE line in eastern India. In the Himalayas, precipitation is heaviest in the western portion of the mountain range; however, precipitation gradually shifts eastward in time. By time $t = 08$ h (0800 UTC) precipitation has reached the Marsyandi network region (small black box in Fig. 10) and re-

mains in some form until after $t = 12$ h. After this time, precipitation area gradually recedes westward. In reality, rainfall started at the Ganpokhara gauge by 0915 UTC with on-off showers throughout the day until 2245 UTC, and the most concentrated rainfall in time occurred prior to 1615 UTC. Thus, the model simulates the overall temporal distribution of precipitation accurately, though the time of storm arrival at the network was one or two hours ahead of observations.

Maximum cloud-liquid water in a vertical column is shown in Fig. 10b. Here, we see that the eastward shift in precipitation along the Himalayas corresponds to the eastward development of cloudiness along the mountains. There also is a northeastward spreading of orographically generated clouds over much of the Tibetan Plateau. Both of these simulated events correspond well to Meteosat-5 observations over the Himalayas and Tibetan Plateau (Fig. 8).

The precipitation feature over eastern India (Fig. 10a) is part of a much longer linear cloud feature over this region. Vertical cross-sections through this line (not shown) reveal that the clouds are low-level and shallow. This too corresponds to features in the IR cloud imagery. For example, in Fig. 8b there is substantial low-level cloudiness over eastern India, running in a quasi-linear fashion from north to south. Although shape and orientation do not match exactly between model and observations, the WINLRG simulation captures the basic character of the observations, including the widening of the line toward the mountains to the north.

Short N-S linear mesoscale cloud features are sometimes observed propagating eastward along the Himalayan barrier in the simulation results. For example, see the small cloud feature jutting south from the network area at $t = 12$ h in Fig. 10b. These features also were noted in the Meteosat-5 (Fig. 8) and TRMM PR (Fig. 9) data. They propagate eastward in concert with the gradual eastward shift in orographically generated clouds over the mountains themselves. These along-barrier mesoscale features could be responsible for precipitation along the northern Indian plains as well as portions of the Marsyandi network.

To understand the behavior of the clouds and precipitation, we now turn to the wind output from the model. Fig. 10c shows surface winds while Fig. 10d shows upper-level winds, at 8 km MSL. The model was initialized with light easterly low-level flow along the central Himalayan barrier, associated with the cyclonic flow around the notch depression. This barrier jet gradually strengthens and extends further east, such that by $t = 12$ h there is well-developed low-level flow from the Bay of Bengal toward the central and western Himalayas. However, it largely remains under 4 km MSL (not shown), with westerly flow aloft. This jet would be expected to feed convection with moisture piped from the Bay of Bengal, and may explain the development and maintenance of the mesoscale low-altitude, along-barrier cloud and precipitation features seen in both the observations and the model. The jet gradually weakens after $t = 12$ h.

The development of this jet is associated with apparent wave breaking and strong surface wind speeds over portions of the central Himalayas and southern Tibetan Plateau. Note, however, that the network region is in a wind speed lull (< 10 m s^{-1}), which is supported by anemometer measurements during snow events. The shallow easterly barrier jet predicted by the model was observed by the 11 February 0000 and 1200 UTC soundings from the Gorakhpur station in northern India (83.37°E, 26.75°N; WMO #42379), with maximum 850 hPa winds reaching 15 m s^{-1} at 1200 UTC. This corresponds well to the model-predicted flow speeds in this area ($\sim$200 km SW of the network, SE of the location of the jet maximum in the model).

Aloft at 8 km MSL, the flow is predominantly westerly (Fig. 10d). However, as time progresses, there is a slight backing of the 8 km MSL wind to WSW. This occurs in concert with the development of significant speed convergence near the central Himalayas at 6 km MSL (not shown), as well as the eastward shift of orographically generated clouds and precipitation along the Himalayan barrier (Fig. 10a–b). Based on the geometry of the Himalayan barrier, it appears that this wind shift is responsible for the eastward shift in cloudiness and precipitation. The Marsyandi network is just west of a major change in the angle of the Himalayas. East of this point, the mountains run roughly W-E, while to the west the barrier is arranged WNW-ESE (Fig. 10). Therefore, a

shift to WSW flow provides a larger angle of incidence on the central Himalayas and should better favor orographic cloud generation along the southward-facing slopes. This also explains why the eastern Himalayas do not see as much cloudiness (and presumably precipitation) from these notch depressions (Figs. 8, 10a–b), as the E-W orientation of the mountains presents a much smaller angle of incidence to winds with strong westerly components. In essence, the evolution of the depression against the unique geometry of the barrier may control the timing and distribution of precipitation.

5. Discussion and conclusions

Observations from a meteorological network suggest that snowfall contributes up to 25–35% of annual precipitation at high elevations ($>$ 3000 m MSL) in the central Himalayas. This percentage increases with altitude and tends to mitigate differences in annual precipitation between very-high-altitude stations ($>$ 4000 m MSL) and lower-elevation ridge stations (3000–4000 m MSL). The snow contribution can be up to 100 cm or more, liquid water equivalent. However, these amounts are strongly modulated by interannual variability, which can exceed 20–30% of annual totals. Low-elevation stations ($<$ 3000 m MSL) stay above 0°C and receive little rain during the winter months (generally $<$ 20 cm over the entire Jan–Mar period).

Major snowfall events in the central Himalayas are primarily caused by Western Disturbances, which are westerly waves trapped and intensified by the unique large-scale topographic features, most notably the notch formed by the Himalayas and Hindu Kush mountains. The interannual variability of these systems is large, and there is some limited evidence that suggests the overall strength of the circumpolar westerly flow, and the placement of the oncoming wave with respect to the Tibetan Plateau (north or south), are factors in the prevalence of these systems during any particular year.

A numerical simulation of a representative snow event suggests that orographic forcing is the dominant factor in precipitation in the central Himalayas. Significant precipitation in this region only occurs when the large-scale flow evolves to a favorable geometry with respect to the mountains. In addition, along-barrier mesoscale precipitation features fed by an easterly barrier jet may play an important role in regional precipitation during these events, especially at lower elevations and along the foothills of the Himalayan range. Characterization of the detailed interactions of this easterly jet, with local cloud and precipitation systems, will be investigated in a forthcoming paper.

Acknowledgements

Downloading and initial processing of the Marsyandi network data were managed by Dr. Jaakko Putkonen of the University of Washington and Tank Ojha of The Himalayan Experience. Dr. Terry Clark of NCAR assisted with the implementation of the numerical model. TRMM data were obtained from the NASA DAAC, Meteosat-5 data from the University of Wisconsin SSEC, and NCEP/NCAR Reanalysis and Indian radiosonde data from the NCAR Mass Storage System. This research was funded in part by NASA-TRMM Grant NAG5-9823 and by NSF Grant EAR-9909498.

References

Barros, A.P., M. Joshi, J. Putkonen, and D.W. Burbank, 2000: A study of the 1999 monsoon rainfall in a mountainous region in central Nepal using TRMM products and rain gauge observations. *Geophys. Res. Lett.*, **27**, 3683–3686.

Barros, A.P. and T.J. Lang, 2003: Monitoring the monsoon in the Himalayas: Observations in central Nepal, June 2001. *Mon. Wea. Rev.*, **131**. No. 7, 1408–1427.

Bruintjes, R.T., T.L. Clark, and W.D. Hall, 1994: Interactions between topographic airflow and cloud/precipitation development during the passage of a winter storm in Arizona. *J. Atmos. Sci.*, **51**, 48–67.

Clark, T.L., 1977: A small-scale numerical model using a terrain-following coordinate transformation. *J. Comput. Phys.*, **24**, 186–215.

———, 1979: Numerical simulations with a three-dimensional cloud model: Lateral boundary condition experiments and multi-cellular severe storm simulations. *J. Atmos. Sci.*, **36**, 2191–2215.

——— and R.D. Farley, 1984: Severe downslope windstorm calculations in two and three spatial dimensions using anelastic interactive grid nesting: A possible mechanism for gustiness. *J. Atmos. Sci.*, **41**, 329–350.

——— and W.D. Hall, 1991: Multi-domain simulations of the time dependent Navier Stokes

equation: Benchmark error analyses of nesting procedures. *J. Comput. Phys.*, **92**, 456–481.

——— and ———, 1996: On the design of smooth, conservative vertical grids for interactive grid nesting with stretching. *J. Appl. Meteor.*, **35**, 1040–1046.

Dey, B. and O. Bhanu Kumar, 1982: An apparent relationship between Eurasian snow cover and advanced period of the Indian summer monsoon. *J. Appl. Meteor.*, **21**, 1929–1932.

———, S.N. Kathuria, and O. Bhanu Kumar, 1985: Himalayan summer snow cover and withdrawal of the Indian summer monsoon. *J. Appl. Meteor.*, **24**, 865–868.

Dickson, R.R., 1984: Eurasian snow cover versus Indian monsoon rainfall—an extension of the Hahn-Shukla results. *J. Climate Appl. Meteor.*, **24**, 171–173.

Fu, C. and J.O. Fletcher, 1985: The relationship between Tibet-tropical ocean thermal contrast and interannual variability of Indian monsoon rainfall. *J. Climate Appl. Meteor.*, **24**, 841–847.

Gupta, A., L.S. Rathore, S.V. Singh, and N. Mendiratta, 1999: Performance of a global circulation model in predicting the winter systems and associated precipitation over North West India during 1994–97. In *The Himalayan Environment*, S.K. Dash and J. Bahadur (Eds.), New Age International, 123–138.

Hahn, D.G. and J. Shukla, 1976: An apparent relationship between Eurasian snow cover and Indian monsoon rainfall. *J. Atmos. Sci.*, **33**, 2461–2462.

Kalnay, E., M. Kanamitsu, R. Kistler, W. Collins, D. Deaven, L. Gandin, M. Iredell, S. Saha, G. White, J. Woollen, Y. Zhu, M. Chelliah, W. Ebisuzaki, W. Higgins, J. Janowiak, K.C. Mo, C. Ropelewski, J. Wang, A. Leetmaa, R. Reynolds, R. Jenne, and D. Joseph, 1996: The NCEP/NCAR 40-year reanalysis project. *Bull. Amer. Meteor. Soc.*, **77**, 437–471.

Kessler, E., 1969: *On the distribution and continuity of water substance in atmospheric circulations*. *Meteor. Monogr.* No. 32, Amer. Meteor. Soc., 84 pp.

Klaassen, G.P. and T.L. Clark, 1985: Dynamics of the cloud-environment interface and entrainment into small cumuli: Two-dimensional simulations in the absence of ambient shear. *J. Atmos. Sci.*, **42**, 2621–2642.

Kummerow, C., W. Barnes, T. Kozu, J. Shiue, and J. Simpson, 1998: The Tropical Rainfall Measuring Mission (TRMM) sensor package. *J. Atmos. Oceanic Technol.*, **15**, 809–816.

Lang, T.J. and A.P. Barros, 2002: An investigation of the onsets of the 1999 and 2000 monsoons in central Nepal. *Mon. Wea. Rev.*, **130**, 1299–1316.

Li, C. and M. Yanai, 1996: The onset and interannual variability of the Asian summer monsoon in relation to land-sea thermal contrast. *J. Climate*, **9**, 358–375.

Ohsawa, T., T. Hayashi, Y. Mitsuta, and J. Matsumoto, 2000: Intraseasonal variation of monsoon activities associated with the rainfall over Bangladesh during the 1995 summer monsoon season. *J. Geophys. Res.*, **105**, 29445–29459.

Ramasastri, K.S., 1999: Snow melt modeling studies in India. In *The Himalayan Environment*, S.K. Dash and J. Bahadur (Eds.), New Age International, 59–70.

Reinking, R.F., J.B. Snider, and J.L. Coen, 2000: Influences of storm-embedded orographic gravity waves on cloud liquid water and precipitation. *J. Appl. Meteor.*, **39**, 733–759.

Shrestha, M.L., 2000: Interannual variation of summer monsoon rainfall over Nepal and its relation to Southern Oscillation Index. *Meteor. Atmos. Phys.*, **75**, 21–28.

Sikka, D.R., 1999: Influence of Himalayas and snow cover on the weather and climate of India—A review. In *The Himalayan Environment*, S.K. Dash and J. Bahadur (Eds.), New Age International, 37–52.

Smolarkiewicz, P.K., 1984: A fully multidimensional positive definite advection transport algorithm with small implicit diffusion. *J. Comput. Phys.*, **54**, 325–362.

——— and T.L. Clark, 1986: The multidimensional positive-definite advection transport algorithm: Further development and applications. *J. Comput. Phys.*, **67**, 396–438.

Ueno, K., R.B. Kayastha, M.R. Chitrakar, O.R. Bajracharya, A.P. Pokhrel, H. Fujinami, T. Kadota, H. Iida, D.P. Manandhar, M. Hattori, T. Yasunari, and M. Nakawo, 2001: Meteorological observations during 1994–2000 at the Automatic Weather Station (GEN-AWS) in Khumbu region, Nepal Himalayas. *Bulletin of Glaciological Research*, **18**, 23–30.